Article:
Adl, H.P., Bennenhei, C., Struve, M. et al. (15 more authors) (2025) Tunable room-temperature polaritons in the very strong coupling regime in quasi-2D Ruddlesden–Popper perovskites. Advanced Optical Materials. ISSN: 2195-1071

https://doi.org/10.1002/adom.202501392

ADVANCED OPTICAL MATERIALS
www.advopticalmat.de

Tunable Room-Temperature Polaritons in the Very Strong Coupling Regime in Quasi-2D Ruddlesden–Popper Perovskites

*Hamid Pashaei Adl, Christoph Bennenhei, Marti Struve, Paulina Peksa, Mateusz Dyksik, Michal Baranowski, Kok Wee Song, Moritz Gittinger, Christoph Lienau, Jonas K. König, Jamie M. Fitzgerald, Naga Prathibha Jasti, Falk Eilenberger, Paulina Plochocka, Ermin Malic, Oleksandr Kyriienko, Martin Esmann, and Christian Schneider**

Layered perovskites are an emergent class of materials, which feature extraordinarily large light–matter coupling, driven by excitons with binding energies significantly beyond the thermal energy at room-temperature. In this work, widely tunable room-temperature cavity exciton polaritons are demonstrated at the cross-over from the strong coupling to the very strong coupling regime in mechanically exfoliated crystals of quasi-2D Ruddlesden–Popper iodide perovskite $(BA)_2(MA)_2Pb_3I_{10}$ embedded in an open microcavity. The coupled exciton-cavity system features a Rabi-splitting up to $\Omega_R \simeq 155$ meV, exceeding the experimentally determined exciton binding energy of $E_b = 100 \pm 10$ meV and thus operates at the onset of the very strong coupling regime, in which the light–matter coupling alters the interaction of electron and hole. This combined experimental-theoretical effort provides a consistent microscopic picture successfully describing the observed peculiar scaling of the Rabi-splitting with an increasing effective cavity length. These findings provide a foundation for future on-chip applications involving tunable polaritonic and nonlinear optical devices based on strongly coupled perovskite systems.

1. Introduction

In recent years, quasi-2D Ruddlesden–Popper (RP) perovskites have gained significant attention in the field of optoelectronics and quantum photonics due to their unique electronic and optical properties.[1–5] Quasi-2D perovskites are of high interest in terms of excitonic effects, tunable bandgaps, high photoluminescence quantum yields, and compositional flexibility.[6–8] As illustrated in **Figure 1a**, in contrast to 3D perovskites, the semiconducting inorganic layer in quasi-2D perovskites is surrounded by insulating organic cations, creating a natural 2D quantum-well (QW) structure. The thickness of this QW is determined by the parameter n,[9] which indicates the number of inorganic sheets forming the QW structure, ranging from $n = 1, 2, 3, \ldots$ to effectively bulk configuration.[9,10] These layered perovskites stand out in

H. P. Adl, C. Bennenhei, M. Struve, M. Gittinger, C. Lienau, M. Esmann, C. Schneider
Institut für Physik, Fakultät V
Carl von Ossietzky Universität Oldenburg
26129 Oldenburg, Germany
E-mail: christian.schneider@uni-oldenburg.de
H. P. Adl
Instituto de Ciencia de Materiales (ICMUV)
Universidad de Valencia
C/ Catedrático José Beltrán, 2, Paterna 46980, Spain

The ORCID identification number(s) for the author(s) of this article can be found under https://doi.org/10.1002/adom.202501392

DOI: 10.1002/adom.202501392

P. Peksa, P. Plochocka
Laboratoire National des Champs Magnétiques Intenses, EMFL, CNRS UPR 3228
Université Grenoble Alpes, Université Toulouse
Grenoble and Toulouse, France
P. Peksa, M. Dyksik, M. Baranowski, P. Plochocka
Department of Experimental Physics
Faculty of Fundamental Problems of Technology
Wroclaw University of Science and Technology
Wroclaw 50370, Poland
K. W. Song
Department of Physics
Xiamen University Malaysia
49300 Sepang, Malaysia
C. Lienau
Center for Nanoscale Dynamics (CENAD)
Carl von Ossietzky Universität Oldenburg
26129 Oldenburg, Germany

the field of van der waals materials due to their high exciton oscillator strengths, composition-adjustability, and exceptionally strong exciton binding energies.[11–13]

The integration of layered perovskites in optical microcavities has proven large potential for the development of advanced quantum photonic devices such as low-threshold lasers[14,15] and polariton lasers based on bosonic condensation.[5,16–18] The strong coupling regime[19–21] has become a pivotal concept in the advancement of cavity quantum electrodynamics, a field focused on the manipulation and control of light at the quantum level. This regime describes the interaction between light (photons) and matter (such as excitons in semiconductors or qubits in quantum circuits). The observation of cavity exciton-polaritons in 2D layered perovskites has been recently reported in a variety of cavity structures, including planar dielectric, metallic, and hybrid cavities.[22–28] However, for quasi-2D lead halide perovskites of phases $n > 1$, the formation of exciton-polaritons at room temperature has been demonstrated primarily in relatively thick flakes (thicker than 400 nm),[29] either embedded within monolithic cavities or even in the absence of external distributed Bragg reflectors (DBRs) or specialized optical cavities.[30] In both configurations, the absence of tunable optical parameters constrains the ability to precisely modulate and strengthen the light–matter interaction.

In this study, we use an open-access optical microcavity to demonstrate the formation of exciton-polaritons with a tunable Rabi-splitting of up to $\Omega_R \simeq 155$ meV, surpassing the threshold for the very strong coupling regime. In the very strong coupling regime, the coupling strength became comparable to the exciton binding energy.[19,31,32] Unlike our earlier study,[5] which relied on quasi-2D flakes with a mixed $n = 3$, 4 phase composition where the $n = 4$ component enabled ultra-low-threshold polariton lasing through effective intracavity pumping, the present work employs pure $n = 3$ phase perovskite flakes. Their higher oscillator strength and superior structural uniformity than mixed phase perovskite flakes make them an ideal platform for probing strong and very strong coupling regimes. Our findings confirm large values of interband matrix elements for optical transitions in RP perovskites, highlighting their promise for polaritonic applications, and display an unusual scaling of the Rabi-splitting in relation to the effective cavity length, which originates from the material-specific field penetration in to the quasi-2D material slab.

J. K. König, J. M. Fitzgerald, E. Malic
Fachbereich Physik
Philipps-Universität
35032 Marburg, Germany

N. P. Jasti
Department of Molecular Chemistry and Materials Science
Weizmann Institute of Science
Rehovot 7610001, Israel

N. P. Jasti
Chemistry and Physics of Materials Unit
JNCASR
Bangalore 560064, India

F. Eilenberger
Fraunhofer-Institute for Applied Optics and Precision Engineering IOF
07745 Jena, Germany

F. Eilenberger
Institute of Applied Physics
Abbe Center of Photonics
Friedrich Schiller Universität Jena
07745 Jena, Germany

F. Eilenberger
Max Planck School of Photonics
07745 Jena, Germany

O. Kyriienko
School of Mathematical and Physical Sciences
University of Sheffield
Sheffield S10 2TN, UK

2. Results and Discussion

The quasi-2D perovskite single crystals with n = 3 phase, $(BA)_2(MA)_{n-1}Pb_nI_{3n+1}$, were synthesized and crystallized using an adapted version of the slow-cooling method[33–35] (see Experimental Section for more details). Figure 1a shows the crystal structure of $(BA)_2(MA)_2Pb_3I_{10}$ (n = 3 phase). It is made up of a triple layer of perovskite inorganic octahedral unit cells composed by $(PbI_6)^-$ units sandwiched between long organic Butylammonium $(BA)^+$ cations, which serve as spacers. The inorganic triple layer is intercalated by short organic Methylammonium $(MA)^+$ cations. Figure 1b shows the photoluminescence (PL), one-photon photoluminescence excitation (PLE) together with reflectance spectra of a $(BA)_2(MA)_2Pb_3I_{10}$ single crystal recorded at $T = 4$K. The PL spectrum exhibits two main features, typical for quasi-2D layered perovskites.[12,36–38] The dominating PL feature ($\simeq$ 2.03 eV) is red-shifted with respect to the resonant excitonic feature ($\simeq$ 2.046 eV) visible in the reflectivity spectrum, that we ascribe it to excitons trapped at extrinsic defects or exciton-polaron formation (LX).[36,39–41] The less intense high-energy PL peak ($\simeq$ 2.046 eV) overlaps with features visible in reflectance and thus is ascribed to the free 1s exciton state (FX). As shown in Figure 1b, we performed PLE measurements to determine the bandgap energy position. As gradual increase in PL intensity is observed in the range of $\simeq$ (2.13–2.17 eV), providing a robust base for estimating the bandgap energy using the Elliot formula,[42] which accounts for transition broadening, as illustrated in the plot. Further details are provided in Section S1 (Supporting Information). The value of the bandgap $E_g \simeq 2.146$ eV (indicated by dashed line) and 1s transition energy ($E_{1s} \simeq 2.046$eV) determine the exciton binding energy of $E_b \simeq 100$ meV (± 10 meV). This value is further corroborated by two-photon PLE measurements and optical response in the high magnetic field presented in Section S1 (Supporting Information). The measured exciton binding energy is also consistent with material-specific calculations using the Wannier equation predicting a value of the same order of magnitude. Further details and data supporting these findings can be found in Section S2 (Supporting Information). Mechanically exfoliated RP perovskite crystals in the $n = 3$ phase were transferred onto a DBR using the dry-gel stamping method.[43] Exfoliation reduces the existence of unwanted hybrid phase formation[44] and leads to strictly flat and thin crystals. Atomic force microscopy (AFM) measurements determined the thickness of the exfoliated flakes to be 224 nm (see **Figure 2a**). The corresponding PL spectrum shown in Figure 2b measured under continuous-wave (CW) laser excitation at 532 nm at ambient conditions manifests a single peak, which can be ascribed to the optical resonance of the exciton at room-temperature.[33]

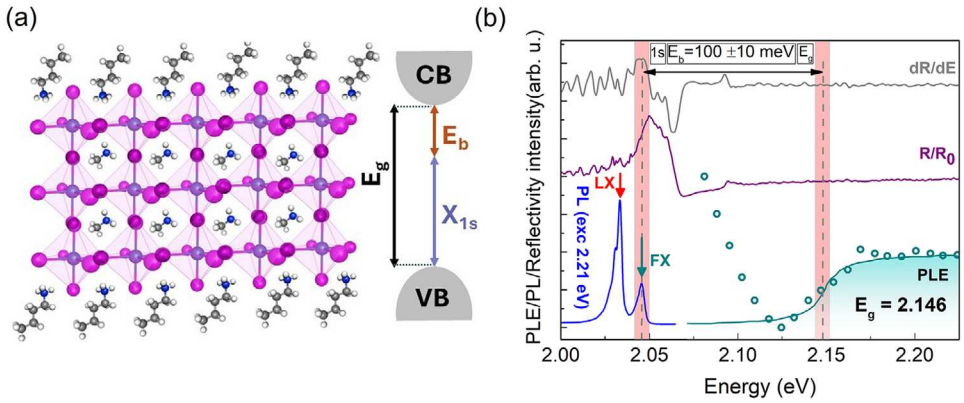

Figure 1. a) The crystal structure of the quasi-2D perovskite single crystals with n = 3 phase, $(BA)_2(MA)_{n-1}Pb_nI_{3n+1}$. This structure is composed of three layers of perovskite inorganic octahedral units. The energy level structure of this material is represented by a diagram that includes the valence band (VB), conduction band (CB), and the electronic band gap (E_g). Additionally, the diagram highlights the 1s exciton optical transition (X_{1s}), and the exciton binding energy (E_b). b) PL (blue line) and reflectance (purple line) spectra for $(BA)_2(MA)_2Pb_3I_{10}$ together with differential reflectivity spectrum (grey line). The dashed lines indicate the energies of 1s excitonic transition and bandgap. Green open points represent the result of PLE monitored on the FX PL peak. The green line is the result of a fit with the Elliot formula (we considered only the band-to-band transitions part with the Sommerfeld factor[42]). The shaded bars indicate the uncertainty of FX and bandgap position (±4 meV and ±6 meV). Measurements are performed at T= 4K.

Despite the enhanced stability of 2D perovskites compared to their 3D counterparts,[45–47] they still experience photobleaching, when exposed to laser excitation in ambient conditions (Figure 2e, blue spheres). To mitigate this issue, we encapsulated the perovskite flakes entirely within two thin (~ 20 nm) layers of hexagonal boron nitride (hBN), effectively preventing both photo-oxidation and moisture absorption.[48] As shown in Figure 2c,d, we transferred both the bare and fully encapsulated flakes onto a DBR (see Experimental Section). The comparative analysis of PL emission stability for both bare and fully encapsulated perovskite flakes is depicted in Figure 2e,f. These figures illustrate the PL stability under CW laser excitation at 532 nm, at low 28.31 W mm^{-2} and relatively high 283.1 W mm^{-2} power densities, respectively. The encapsulated perovskite flakes (green symbols) show

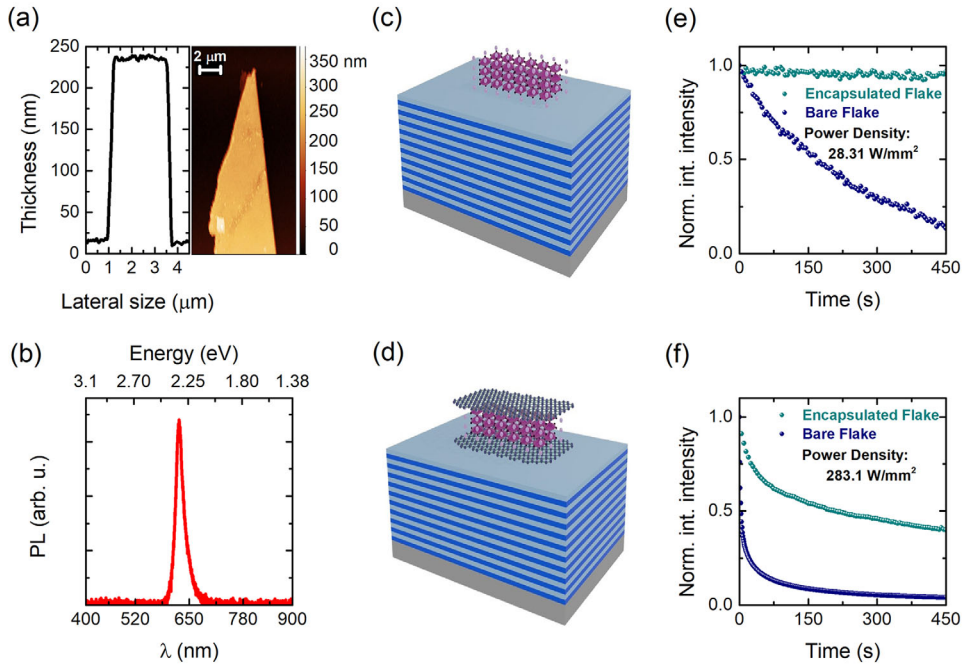

Figure 2. a) Atomic force microscopy (AFM) image of an exfoliated $n = 3$ phase quasi-2D Ruddlesden-Popper perovskite flake and the corresponding height profile obtained after deposition on a bottom DBR. b) The photoluminescence (PL) spectrum of an exfoliated flake of $(BA)_2(MA)_2Pb_3I_{10}$ obtained under CW excitation at 532 nm in ambient conditions. Panels (c) and (d) schematically depict the exfoliated bare and encapsulated flakes of $(BA)_2(MA)_2Pb_3I_{10}$ deposited atop a DBR (blue: TiO_2, grey: SiO_2). The encapsulation process involves placing a perovskite flake between two thin (~ 10 nm) hBN flakes. Panels (e) and (f) depict a comparative analysis of the PL emission from bare (blue symbols) and encapsulated (green symbols) perovskite flakes over time, under power densities of 28.31 W mm^{-2} and 283.1 W mm^{-2}, respectively.

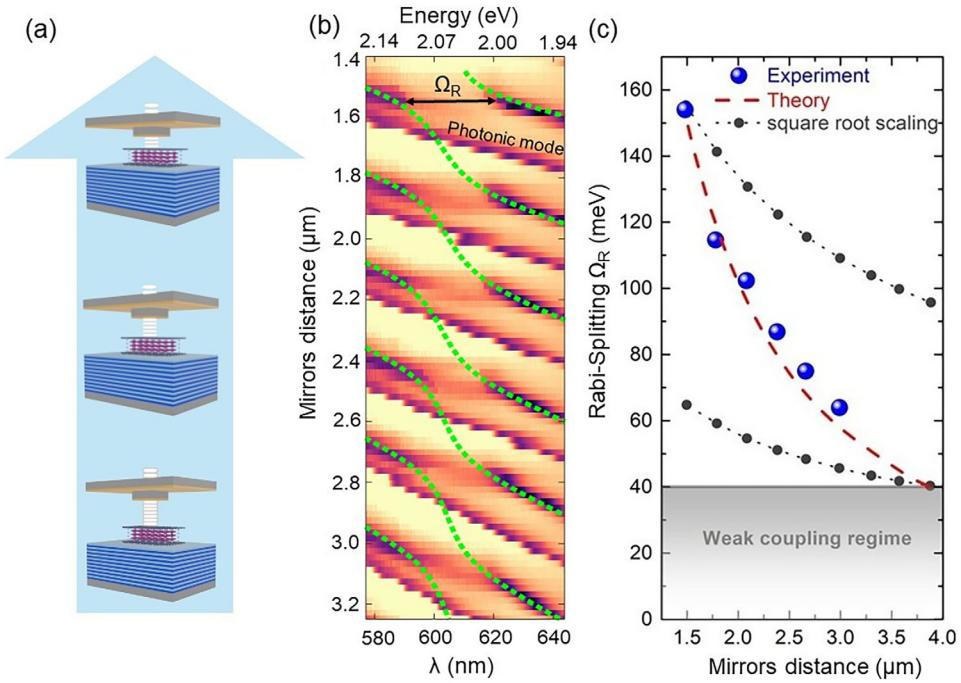

Figure 3. a) Schematic of the optical microcavity sample, which comprises a bottom DBR and a metallic top mirror, with flakes embedded within the microcavity. The cavity length was progressively reduced from bottom to top by moving the bottom DBR closer to the top mirror. b) White light reflectivity spectra, extracted at the in-plane wavevector $k_{||} = 0$. The mirrors distance was gradually reduced from $L_{cav} = 3.24$ μm to $L_{cav} = 1.40$ μm. The green dashed lines correspond to fits based on the coupled oscillator model. c) Rabi-splitting as a function of mirrors distance, corresponding to each anti-crossing in panel (b) from successive longitudinal cavity modes. Blue spheres represent the experimental data, while the red dashed curve is based on our adapted scaling model. Black circles with dotted curves represent the typical square root dependence of Rabi-splitting on cavity length (with largest and smallest air gap values serving as a reference).

significantly enhanced stability compared to their bare (blue symbols) counterparts, emphasizing the importance of encapsulation in preserving the perovskite material's integrity under light exposure in ambient conditions. By limiting the excitation power density, it is possible to prevent photobleaching of the PL completely (see green spheres in Figure 2e).

Figure 3a shows the implementation of our sample based on an open-access optical cavity setup.[49] In this configuration, the top cavity reflector is a planar gold mirror consisting of a 35 nm gold film deposited on a mesa structure. Two mirrors are mounted on separate xyz piezo stacks, forming an air-gapped Fabry–Perot resonator. Unlike monolithic cavity designs, this setup allows for full flexibility in tuning the cavity resonance by adjusting the distance between the mirrors and their relative in-plane positioning. To observe cavity exciton-polaritons in quasi-2D perovskites, we conducted white light (WL) reflectivity measurements under ambient conditions, and progressively reduced the cavity length from bottom to top by moving the bottom DBR closer to the top mirror. As depicted in Figure 3b, this process involved gradually decreasing the mirrors distance from $L_{cav} = 3.24$ μm to $L_{cav} = 1.40$ μm and capturing the reflectivity spectra at normal incidence ($k_{||} = 0$). Throughout this process, we observed a clear anti-crossing behavior corresponding to successive longitudinal cavity modes, with the Rabi-splitting systematically increasing as the cavity length was reduced. This is best seen by inspecting reflectivity spectra at fixed gap distance, as shown in Figure S4 Section S3 (Supporting Information). Since we probe white light reflectivity spectra from a sample area larger than the perovskite flake, we observe additional bare photonic modes from the empty parts of the cavity appearing as straight lines in Figure 3b (Section S4 for details, Supporting Information). The data in Figure 3b were obtained from momentum-resolved WL reflectivity spectra acquired during a long range cavity distance scan and evaluated using the method shown in **Figure** 4. The Rabi-splitting at each anti-crossing was determined using fits from a two-coupled oscillator model (represented by green dotted lines) and re-evaluated with double Lorentzian fits for more precise estimations (refer to Sections S5 and S3, Supporting Information). Additionally, the experimental results were further validated by comparison with transfer matrix simulations, utilizing dielectric functions from reference[50] (see Section S4, Supporting Information). These calculated values are plotted as a function of the mirrors distance in Figure 3c. In this plot, a shaded region is visible, where losses exceed the coherent coupling rate, and the system crosses over to the weak coupling regime. This is determined based on the visibility criterion, which compares the magnitude of the Rabi-splitting with the linewidth of the uncoupled oscillators. This condition is expressed as $\Omega_R > (\gamma_c + \gamma_x)/2$,[51,52] where $\gamma_c \simeq 20$ meV represents the linewidth of the cavity mode, and $\gamma_x \simeq 60$ meV corresponds to the exciton resonance linewidth (refer to Section S5, Supporting Information). Interestingly, the dependency of the Rabi-splitting on cavity length does not follow the expected square root relationship $\Omega_R \propto 1/\sqrt{L_{cav}}$ (see Section S4, Supporting Information, for a detailed formula)

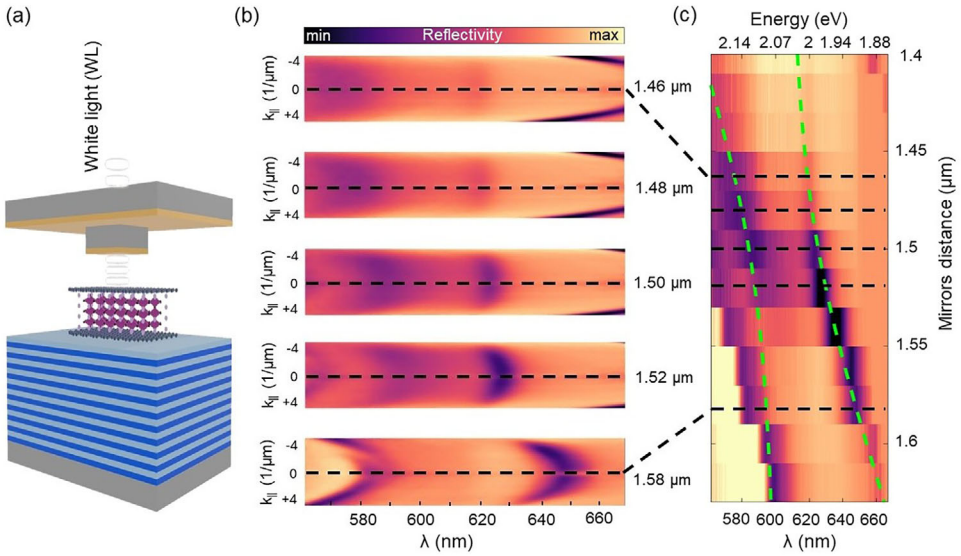

Figure 4. a) Schematic of the optical cavity at its minimum possible length. b) Angle-resolved white light (WL) spectra, showing the systematic increase in cavity length from top to bottom by approximately 120 nm. c) Cross-sectional profiles of the angle-resolved WL spectra, taken at the in-plane wavevector $k_{||} = 0$. The green dashed lines correspond to fits based on the coupled oscillator model.

that is typically observed in the strong coupling regime.[53–55] This deviation indicates that the system is influenced by additional factors beyond the conventionally applied most simple model.

Due to the large optical transition dipole moment for RP perovskites the effects of cavity mode profile and electric field penetration into the material become crucial. The field penetration depends on an effective mode volume, and thus changes with a mode number m, leading to a modified scaling of the light–matter coupling strength. We account for the spatial profile of modes within the sample, where the electric field magnitude decreases for larger mode numbers m, as well as the penetration depth (see Section S6 for the details, Supporting Information). This leads to a faster decrease of the Rabi-splitting with increasing cavity length, as compared to the simple square root scaling. For cavity-based devices relying on strong or very strong coupling regimes, this finding highlights the importance of optimizing the cavity length and mode structure to maintain sufficient field overlap and coupling strength, especially in cavity designs where tuning is limited or absent. Practically, this could involve engineering the DBRs to minimize penetration depth, selecting cavity geometries that confine the field more effectively within the perovskite layer, or employing hybrid cavity architectures that compensate for mode dilution at larger lengths. We propose a model for describing scaling behavior of Rabi-splitting Ω_m shown in Equation (1), which aligns well with the experimental data represented by the blue spheres in Figure 3c. It reads

$$\Omega_m = \frac{\tilde{A}}{L_{\mathrm{cav}}^{3/2}}\left(1 - \mathrm{e}^{-\tilde{\alpha} d L_{\mathrm{cav}}}\right), \tag{1}$$

where Ω_m is inversely proportional to $L_{\mathrm{cav}}^{3/2}$, and additionally influenced by an exponential term dependent on the perovskite thickness (d) and cavity length (L_{cav}). The empirically derived parameters $\tilde{A}$ and $\tilde{\alpha}$ are inferred to achieve the best fit. The red dashed curve in Figure 3c represents the optimal set of parameters $\tilde{A} = 352$ meV μm$^{3/2}$ and $\tilde{\alpha} = 9.02$ 1/ μm^2, where the perovskite flake thickness is 220 nm. To provide physical context for the empirical parameters in Equation (1), we interpret $\tilde{A}$ as an effective coupling coefficient that reflects the strength of light–matter interaction in the system, incorporating contributions from the exciton oscillator strength and the spatial normalization of the cavity photon mode. The parameter $\tilde{\alpha}$, in contrast, characterizes the effective attenuation of the cavity field into the perovskite layer and governs how the coupling strength evolves with changes in perovskite thickness and cavity length. Specifically, $\tilde{\alpha}$ originates from the exponential decay constant of the cavity mode field profile and reflects the penetration depth of the optical field into the material. The dependence is also supported by numerical profiles of electric field penetration inside the material slab. These parameters are therefore not arbitrary fitting coefficients, but compact representations of the underlying spatial and spectral dependencies of exciton–photon coupling in the cavity system, as detailed in the Note S6 (Supporting Information).

Figure 4a showcases our device and exemplary raw data underlying Figure 3, with the cavity length optimized to be as short as possible. Figure 4b presents the results of a cavity tuning series, where the cavity length was systematically increased from top to bottom by approximately 120 nm. This variation was achieved by adjusting the mirrors distance, and we recorded angle-resolved WL spectra throughout this process using a Fourier imaging geometry.[49] For smaller cavity lengths, the optical modes shift toward shorter wavelengths. The panels show the clear formation of the upper polariton branch (UPB) and the lower polariton branch (LPB) when the optical mode couples to the exciton, with the lower polariton not crossing the exciton resonance. Notably, as the cavity approaches the exciton resonance, the parabolic dispersion of the LPB shows a significant flattening, indicating a substantially larger excitonic fraction (50%) near

zero-detuning than far red-detuned case (38%) (bottom most spectrum in Figure 4b, see also Note S5, Supporting Information, for Hopfield coefficients details). Figure 4c shows cross-sectional slices of these spectra extracted at the in-plane wavevector $k_{||} = 0$, where we observe distinct anti-crossing behavior at the chosen mirrors distance of 1.5 µm. We determine a light-matter coupling strength of $g = 77.5$ meV, corresponding to a Rabi-splitting energy of $\Omega_R = 2g \simeq 155$ meV. As the cavity length decreases and the coupling strength increases, the system enters the very strong coupling regime when the Rabi-splitting energy exceeds the exciton binding energy of quasi-2D perovskites,[19,31,32] leading to substantial changes in the electron-hole interaction, since the photon becomes strongly coupled also to higher energy exciton states and the electron-hole continuum.[56] In our case, the Rabi-splitting ($\Omega_R \simeq 155$) exceeds the excitonic binding energy of 100 meV and clearly pin-points very strong coupling conditions. In this regime, the system can exhibit highly non-linear behavior, with polariton states becoming more dominant than either the original exciton or photon states.[19,57] The hybridization between light and matter is expected to become more intricate, potentially leading to profound modification of intrinsic excitonic properties of the material. Theoretical studies suggest that such conditions could allow hybridization between the whole Rydberg series of s-type excitons and the electron–hole continuum. This may, in turn, alter the exciton wavefunction and lead to observable deviations in polariton energy, light–exciton composition, scattering behavior, and magneto-optical properties, beyond what is captured by the standard one-exciton–one-photon Hopfield model. These possibilities offer an exciting direction for future exploration in strongly coupled perovskite systems.

To place our work in a broader context, it is worth noting that various material systems, such as GaAs quantum wells, have been widely studied in pursuit of unconventional light–matter coupling regimes.[19,31] However, when compared to traditional II-IV and III-V semiconductors, quasi-2D perovskites offer significant advantages, particularly for reaching unconventional coupling regimes such as very strong coupling. Mainly, II-IV and III-V based excitons are characterized by relatively small binding energies, which limits their operation to low temperatures and constrains their applicability in regimes where coupling strength approaches or exceeds the exciton binding energy in elevated temperatures. In contrast, quasi-2D perovskites exhibit much larger exciton binding energies and exceptionally strong oscillator strengths, enabling coupling strengths that can reach or surpass binding energy even at room temperature. This makes quasi-2D perovskites an especially promising platform for accessing unconventional light–matter coupling regimes. Furthermore, their ambient stability, tunability through compositional and structural engineering, and compatibility with low-cost fabrication techniques make them an accessible and versatile system for exploring unconventional light–matter interaction regimes.

3. Conclusion

Quasi-2D lead-based halide perovskites are highly suitable for polaritonic studies at room-temperature. We demonstrate the emergence of room-temperature cavity exciton-polaritons in $(BA)_2(MA)_2Pb_3I_{10}$ embedded in an optical microcavity. The system exhibits spectrally tunable polaritons and an unconventional scaling of the Rabi-splitting with the effective cavity length. The light-matter coupling strength can further be tuned, ultimately reaching the very strong coupling regime. In conjunction with the recent first demonstration of polariton condensation of quasi-2D RP perovskites at room-temperature,[5] these results pave the way for vast opportunities in the development of low threshold polariton lasers, ultrafast polariton switches, and nonlinear optical devices on a chip.

4. Experimental Section

Perovskite Synthesis: Butylammonium, $C_4H_9NH_3$ (BA) methylammonium, CH_3NH_3 (MA) lead iodide $(BA)_2(MA)_2Pb_3I_{10}$ (C_4N_3) was crystallized using the slow-cooling method with minor modifications.[33,34] (see Section S7, Supporting Information, for detailed procedure)

Sample Preparation: The bottom mirrors were fabricated by RF sputtering 10 alternating layers of SiO_2 (107nm) and TiO_2 (67nm) layers, terminating in a SiO_2 layer. The upper mirror is fabricated by depositing a 35 nm gold layer on a 1.5 mm thick glass substrate that features a $100 \times 100 \times 100\ \mu m^3$ mesa structure, which is fabricated by removing the surrounding 100 μm of material prior to the gold deposition.

$(BA)_2(MA)_2Pb_3I_{10}$ single crystals were exfoliated using the scotch tape method, followed by dry stamping with PDMS. The process began with the deposition of a 10 nm thick hBN bottom layer (2D Semiconductors) on a substrate heated to 100°C, with a 5-minute contact time. Next, the quasi-2D RP LHP flake was placed on the substrate at 20°C, with a 20-minute contact time using PDMS GelPak grade zero, pre-baked at 85°C for 4 hours. Finally, another 10 nm thick hBN flake was applied on top to fully encapsulate the structure, with the substrate at 20°C and a 20-minute contact time. All preparation was conducted under yellow light, and the finished samples were stored in the dark under a nitrogen atmosphere.

Optical Setup: Section S8 (Supporting Information) provides a schematic of the experimental setup. A continuous wave (CW) 532 nm laser is tightly focused onto the sample using a 50X Mitutoyo Plan Apo NIR HR microscope objective with a numerical aperture of 0.65. This objective also serves to collect the photoluminescence (PL) emission and measure white light (WL) reflectivity, using a Thorlabs SLS301 light source. Further details on the open cavity setup can be found in references.[49,58] The emitted/reflected light is analyzed using an Andor iKon-M 934 CCD camera connected to a monochromator (Andor SR-500i-A-SIL). For angle-resolved measurements, the back-focal plane of the objective is imaged onto the monochromator input with a total magnification of 75X, allowing for precise angular analysis of the emitted light.

Supporting Information

Supporting Information is available from the Wiley Online Library or from the author.

Acknowledgements

The authors acknowledge support by the German research foundation (DFG) via the project SCHN1376 13.1. Financial support by the Niedersächsisches Ministerium für Wissenschaft und Kultur ("DyNano" and Wissenschaftsraum "ElLiKo" (C.L. and C.S.)) is gratefully acknowledged. O.K. and K.W.S. acknowledge the support from UK EPSRC Awards No. EP/X017222/1. Also, K.W.S. was supported by Xiamen University Malaysia Research Fund (Grant No: XMUMRF/2025-C15/IPHY/0005). M.E. acknowledges funding by the University of Oldenburg through a Carl von Ossietzky Young Researchers' Fellowship. H.P.A. acknowledges funding by the University of Valencia through the Margarita Salas grant (MS21-181) for the training of young doctors. P.P. acknowledges support from the National Science Centre Poland within the MAESTRO

(2020/38/A/ST3/00214) program. M.D. acknowledges support from the National Science Centre Poland, Grant No. 2023/51/B/ST5/02908. M.B. acknowledges support from the National Science Centre Poland within the OPUS LAP grant (2021/43/I/ST3/01357). E. M. acknowledges funding from the DFG via the regular projects 524612380 and 504846924. The authors acknowledge Dr. Sigalit Aharon (Weizmann Inst. and Princeton Univ.) for sample selection, logistics and guidance for their handling and preparation for measurements.

Open access funding enabled and organized by Projekt DEAL.

Conflict of Interest

The authors declare no conflict of interest.

Data Availability Statement

The data that support the findings of this study are available from the corresponding author upon reasonable request.

Keywords

exciton-polariton, open optical microcavity, quasi-2D perovskites, very strong coupling regime

Received: May 2, 2025
Revised: August 22, 2025
Published online:

[1] M. D. Smith, B. A. Connor, H. I. Karunadasa, *Chem. Rev.* **2019**, *119*, 3104.
[2] S. Gorji, M. Krečmarová, A. Molina, M. C. Asensio, A. F. Gualdrón-Reyes, J. Rodríguez-Romero, H. Pashaei-Adl, R. Canet-Albiach, L. Schio, M. Tormen, L. Floreano, I. Mora-Seró, J. P. M. Pastor, J. F. Sánchez-Royo, G. M. Matutano, *Appl. Phys. Rev.* **2024**, *11*, 2.
[3] R. Canet-Albiach, M. Krecmarova, J. B. Bailach, A. F. Gualdrón-Reyes, J. Rodríguez-Romero, S. Gorji, H. Pashaei-Adl, I. Mora-Seró, J. P. Martinez Pastor, J. F. Sánchez-Royo, G. Muñoz-Matutano, *Nano Lett.* **2022**, *22*, 7621.
[4] J.-C. Blancon, J. Even, C. C. Stoumpos, M. G. Kanatzidis, A. D. Mohite, *Nat. Nanotechnol.* **2020**, *15*, 969.
[5] M. Struve, C. Bennenhei, H. P. Adl, K. W. Song, H. Shan, N. Mathukhno, J.-C. Drawer, F. Eilenberger, N. P. Jasti, D. Cahen, O. Kyriienko, C. Schneider, M. Esmann, *arXiv preprint arXiv:2408.13677* **2024**.
[6] L. Dou, A. B. Wong, Y. Yu, M. Lai, N. Kornienko, S. W. Eaton, A. Fu, C. G. Bischak, J. Ma, T. Ding, N. S. Ginsberg, L.-W. Wang, A. P. Alivisatos, P. Yang, *Science* **2015**, *349*, 1518.
[7] Y. Chen, Y. Sun, J. Peng, J. Tang, K. Zheng, Z. Liang, *Adv. Mater.* **2018**, *30*, 1703487.
[8] J.-C. Blancon, H. Tsai, W. Nie, C. C. Stoumpos, L. Pedesseau, C. Katan, M. Kepenekian, C. M. M. Soe, K. Appavoo, M. Y. Sfeir, S. Tretiak, P. M. Ajayan, M. G. Kanatzidis, J. Even, J. J. Crochet, A. D. Mohite, *Science* **2017**, *355*, 1288.
[9] K. Leng, W. Fu, Y. Liu, M. Chhowalla, K. P. Loh, *Nat. Rev. Mater.* **2020**, *5*, 482.
[10] A. G. Ricciardulli, S. Yang, J. H. Smet, M. Saliba, *Nat. Mater.* **2021**, 1.
[11] J. J. Thompson, M. Dyksik, P. Peksa, K. Posmyk, A. Joki, R. Perea-Causin, P. Erhart, M. Baranowski, M. A. Loi, P. Plochocka, E. Malic, *Adv. Energy Mater.* **2024**, *14*, 2304343.
[12] M. Dyksik, S. Wang, W. Paritmongkol, D. K. Maude, W. A. Tisdale, M. Baranowski, P. Plochocka, *J. Phys. Chem. Lett.* **2021**, *12*, 1638.
[13] M. Dyksik, M. Baranowski, J. J. Thompson, Z. Yang, M. R. Medina, M. A. Loi, E. Malic, P. Plochocka, *Adv. Energy Mater.* **2024**, 2404769.
[14] C. Wang, G. Dai, J. Wang, M. Cui, Y. Yang, S. Yang, C. Qin, S. Chang, K. Wu, Y. Liu, H. Zhong, *Nano Lett.* **2022**, *22*, 1338.
[15] S. Reitzenstein, T. Heindel, C. Kistner, A. Rahimi-Iman, C. Schneider, S. Höfling, A. Forchel, *Appl. Phys. Lett.* **2008**, *93*, 6.
[16] A. Kavokin, T. C. Liew, C. Schneider, P. G. Lagoudakis, S. Klembt, S. Hoefling, *Nat. Rev. Phys.* **2022**, *4*, 435.
[17] C. Bennenhei, H. Shan, M. Struve, N. Kunte, F. Eilenberger, J. Ohmer, U. Fischer, S. Schumacher, X. Ma, C. Schneider, M. Esmann, *ACS Photonics* **2024**.
[18] S. Betzold, M. Dusel, O. Kyriienko, C. P. Dietrich, S. Klembt, J. Ohmer, U. Fischer, I. A. Shelykh, C. Schneider, S. Hofling, *ACS Photonics* **2019**, *7*, 384.
[19] S. Brodbeck, S. De Liberato, M. Amthor, M. Klaas, M. Kamp, L. Worschech, C. Schneider, S. Höfling, *Phys. Rev. Lett.* **2017**, *119*, 027401.
[20] H. Shan, I. Iorsh, B. Han, C. Rupprecht, H. Knopf, F. Eilenberger, M. Esmann, K. Yumigeta, K. Watanabe, T. Taniguchi, S. Klembt, S. Höfling, S. Tongay, C. Antón-Solanas, I. A. Shelykh, C. Schneider, *Nat. Commun.* **2022**, *13*, 3001.
[21] C. Schneider, M. M. Glazov, T. Korn, S. Höfling, B. Urbaszek, *Nat. Commun.* **2018**, *9*, 2695.
[22] J. Wang, R. Su, J. Xing, D. Bao, C. Diederichs, S. Liu, T. C. Liew, Z. Chen, Q. Xiong, *ACS Nano* **2018**, *12*, 8382.
[23] A. Fieramosca, L. De Marco, M. Passoni, L. Polimeno, A. Rizzo, B. L. Rosa, G. Cruciani, L. Dominici, M. De Giorgi, G. Gigli, L. C. Andreani, D. Gerace, D. Ballarini, D. Sanvitto, *Acs Photonics* **2018**, *5*, 4179.
[24] N. H. M. Dang, D. Gerace, E. Drouard, G. Trippé-Allard, F. Lédée, R. Mazurczyk, E. Deleporte, C. Seassal, H. S. Nguyen, *Nano Lett.* **2020**, *20*, 2113.
[25] M. Laitz, A. E. Kaplan, J. Deschamps, U. Barotov, A. H. Proppe, I. García-Benito, A. Osherov, G. Grancini, D. W. deQuilettes, K. A. Nelson, M. G. Bawendi, V. Bulović, *Nat. Commun.* **2023**, *14*, 2426.
[26] L. Polimeno, G. Lerario, M. De Giorgi, L. De Marco, L. Dominici, F. Todisco, A. Coriolano, V. Ardizzone, M. Pugliese, C. T. Prontera, V. Maiorano, A. Moliterni, C. Giannini, V. Olieric, G. Gigli, D. Ballarini, Q. Xiong, A. Fieramosca, D. D. Solnyshkov, G. Malpuech, D. Sanvitto, *Nat. Nanotechnol.* **2021**, *16*, 1349.
[27] M. Kedziora, M. Krol, P. Kapuscinski, H. Sigursson, R. Mazur, W. Piecek, J. Szczytko, M. Matuszewski, A. Opala, B. Pietka, *Nanophotonics* **2024**, *13*, 2491.
[28] I. Georgakilas, D. Tiede, D. Urbonas, C. Bujalance, L. Caliò, R. Mirek, V. Oddi, R. Tao, D. N. Dirin, G. Rainò, S. C. Boehme, J. F. Galisteo-López, R. F. Mahrt, M. V. Kovalenko, H. Miguez, T. Stöferle, *arXiv preprint arXiv:2408.10667* **2024**.
[29] A. Fieramosca, R. Mastria, K. Dini, L. Dominici, L. Polimeno, M. Pugliese, C. T. Prontera, L. De Marco, V. Maiorano, F. Todisco, D. Ballarini, M. De Giorgi, G. Gigli, T. C. H. Liew, D. Sanvitto, *Nano Lett.* **2024**, *24*, 8240.
[30] C. Ouyang, Y. Li, X. Fu, Z. Zeng, L. Huang, S. Liu, X. Wang, T. Gao, A. Pan, *Appl. Phys. Lett.* **2020**, *117*, 22.
[31] H. Zhang, N. Y. Kim, Y. Yamamoto, N. Na, *Phys. Rev. B: Condens. Matter Mater. Phys.* **2013**, *87*, 115303.
[32] J. Khurgin, *Solid State Commun.* **2001**, *117*, 307.
[33] C. C. Stoumpos, D. H. Cao, D. J. Clark, J. Young, J. M. Rondinelli, J. I. Jang, J. T. Hupp, M. G. Kanatzidis, *Chem. Mater.* **2016**, *28*, 2852.
[34] S. Aharon, D. R. Ceratti, N. P. Jasti, L. Cremonesi, Y. Feldman, M. A. C. Potenza, G. Hodes, D. Cahen, *Adv. Funct. Mater.* **2022**, *32*, 2113354.
[35] N. P. Jasti, I. Levine, Y. Feldman, G. Hodes, S. Aharon, D. Cahen, *Proc. Natl. Acad. Sci. USA* **2024**, *121*, e2316867121.
[36] K. Posmyk, N. Zawadzka, Ł. Kipczak, M. Dyksik, A. Surrente, D. K. Maude, T. Kazimierczuk, A. Babinski, M. R. Molas, W. Bumrungsan, C. Chooseng, W. Paritmongkol, W. A. Tisdale, M. Baranowski, P. Plochocka, *J. Am. Chem. Soc.* **2024**, *146*, 4687.

[37] K. Posmyk, M. Dyksik, A. Surrente, D. K. Maude, N. Zawadzka, A. Babiński, M. R. Molas, W. Paritmongkol, M. Maczka, W. A. Tisdale, P. Plochocka, M. Baranowski, *Adv. Opt. Mater.* **2024**, *12*, 2300877.
[38] K. Posmyk, N. Zawadzka, M. Dyksik, A. Surrente, D. K. Maude, T. Kazimierczuk, A. Babinski, M. R. Molas, W. Paritmongkol, M. Maczka, William A. Tisdale, P. Plochocka, M. Baranowski, *J. Phys. Chem. Lett.* **2022**, *13*, 4463.
[39] D. B. Straus, S. Hurtado Parra, N. Iotov, J. Gebhardt, A. M. Rappe, J. E. Subotnik, J. M. Kikkawa, C. R. Kagan, *J. Am. Chem. Soc.* **2016**, *138*, 13798.
[40] S. Neutzner, F. Thouin, D. Cortecchia, A. Petrozza, C. Silva, A. R. Srimath Kandada, *Phys. Rev. Mater.* **2018**, *2*, 064605.
[41] S. Hurtado Parra, D. B. Straus, B. T. Fichera, N. Iotov, C. R. Kagan, J. M. Kikkawa, *ACS nano* **2022**, *16*, 21259.
[42] D. Campi, C. Coriasso, *Phys. Rev. B* **1995**, *51*, 10719.
[43] A. Castellanos-Gomez, M. Buscema, R. Molenaar, V. Singh, L. Janssen, H. S. Van Der Zant, G. A. Steele, *2D Mater.* **2014**, *1*, 011002.
[44] B. Dhanabalan, A. Castelli, M. Palei, D. Spirito, L. Manna, R. Krahne, M. Arciniegas, *Nanoscale* **2019**, *11*, 8334.
[45] T. L. Leung, I. Ahmad, A. A. Syed, A. M. C. Ng, J. Popović, A. B. Djurišić, *Commun. Mater.* **2022**, *3*, 63.
[46] P. Liu, S. Yu, S. Xiao, *Sustainable Energy Fuels* **2021**, *5*, 3950.
[47] X. Li, J. M. Hoffman, M. G. Kanatzidis, *Chem. Rev.* **2021**, *121*, 2230.
[48] M. Seitz, P. Gant, A. Castellanos-Gomez, F. Prins, *Nanomaterials* **2019**, *9*, 1120.
[49] L. Lackner, M. Dusel, O. A. Egorov, B. Han, H. Knopf, F. Eilenberger, S. Schröder, K. Watanabe, T. Taniguchi, S. Tongay, C. Anton-Solanas, S. Höfling, C. Schneider, *Nat. Commun.* **2021**, *12*, 4933.
[50] B. Song, J. Hou, H. Wang, S. Sidhik, J. Miao, H. Gu, H. Zhang, S. Liu, Z. Fakhraai, J. Even, J.-C. Blancon, A. D. Mohite, D. Jariwala, *ACS Mater. Lett.* **2020**, *3*, 148.
[51] D. Zheng, S. Zhang, Q. Deng, M. Kang, P. Nordlander, H. Xu, *Nano Lett.* **2017**, *17*, 3809.
[52] H. Shan, Z. Liu, X. Wang, F. Lin, Z. Liu, B. Shen, J. Lou, X. Zhu, P. M. Ajayan, Z. Fang, *Laser Photonics Rev.* **2020**, *14*, 2000233.
[53] L. C. Andreani, G. Panzarini, J.-M. Gérard, *Phys. Rev. B* **1999**, *60*, 13276.
[54] R. Chikkaraddy, B. De Nijs, F. Benz, S. J. Barrow, O. A. Scherman, E. Rosta, A. Demetriadou, P. Fox, O. Hess, J. J. Baumberg, *Nature* **2016**, *535*, 127.
[55] S. Hou, L. Y. Tobing, X. Wang, Z. Xie, J. Yu, J. Zhou, D. Zhang, C. Dang, P. Coquet, B. K. Tay, M. D. Birowosuto, E. H. T. Teo, H. Wang, *Adv. Opt. Mater.* **2019**, *7*, 1900857.
[56] J. Levinsen, G. Li, M. M. Parish, *Phys. Rev. Res.* **2019**, *1*, 033120.
[57] D. Citrin, J. Khurgin, *Phys. Rev. B* **2003**, *68*, 205325.
[58] L. Lackner, O. A. Egorov, A. Ernzerhof, C. Bennenhei, V. N. Mitryakhin, G. Leibeling, F. Eilenberger, S. A. Tongay, U. Peschel, M. Esmann, C. Schneider, *arXiv preprint arXiv:2406.05214* **2024**.